Contents lists available at ScienceDirect

Materials Today Physics

Anomalous behavior of the quasi-one-dimensional quantum material Na$_2$OsO$_4$ at high pressure

HPSTAR
717-2019

R. Sereika [a, *], K. Yamaura [b], Y. Jia [c], S. Zhang [c], C. Jin [c, d, e], H. Yoon [f], M.Y. Jeong [f], M.J. Han [f, g], D.L. Brewe [h], S.M. Heald [h], S. Sinogeikin [i, k], Y. Ding [a, **], H.-k. Mao [a, i, j]

[a] Center for High Pressure Science and Technology Advanced Research, Beijing, 100094, China
[b] National Institute for Materials Science, 1-1 Namiki, Tsukuba, Ibaraki, 305-0044, Japan
[c] Institute of Physics, Chinese Academy of Sciences, Beijing, 100190, China
[d] School of Physical Science, University of Chinese Academy of Sciences, Beijing, 100190, China
[e] Collaborative Innovation Center of Quantum Matter, Beijing, 100084, China
[f] Department of Physics, KAIST, 291 Daehak-ro, Yuseong-gu, Daejeon, 34141, Republic of Korea
[g] KAIST Institute for the NanoCentury, Korea Advanced Institute of Science and Technology, Daejeon, 305-701, Republic of Korea
[h] X-ray Science Division, Advanced Photon Source, Argonne National Laboratory, 9700 South Cass Avenue, Argonne, IL, 60439, USA
[i] HPCAT, Geophysical Laboratory, Carnegie Institution of Washington, 9700 South Cass Avenue, Argonne, IL, 60439, USA
[j] Geophysical Laboratory, Carnegie Institution of Washington, Washington, DC, 20015, USA
[k] DACTools LLC, Naperville, IL, 60565, USA

ARTICLE INFO

ABSTRACT

Na$_2$OsO$_4$ is an unusual quantum material that, in contrast to the common 5d^2 oxides with spins = 1, owns a magnetically silent ground state with spin = 0 and a band gap at Fermi level, attributed to a distortion in the OsO$_6$ octahedral sites. In this semiconductor, our low-temperature electrical transport measurements indicate an anomaly at 6.3 K with a power-law behavior inclining through the semiconductor-to-metal transition observed at 23 GPa. Even more peculiarly, we discover that before this transition, the material becomes more insulating instead of merely turning into a metal according to the conventional wisdom. To investigate the underlying mechanisms, we applied experimental and theoretical methods to examine the electronic and crystal structures comprehensively and conclude that the enhanced insulating state at high pressure originates from the enlarged distortion of the OsO$_6$. It is such a distortion that widens the band gap and decreases the electron occupancy in Os's t_{2g} orbital through an interplay of the lattice, charge, and orbital in the material, which is responsible for the changes observed in our experiments.

The structure of Na$_2$OsO$_4$ is characteristic of quasi-one-dimensional anisotropy, reflecting a notable chain structure in which each chain comprises edge-shared OsO$_6$ octahedra [1,2]. In such a system, Fermi liquid (FL) theory no longer applies because of the strongly correlated electronic behavior confined in the narrow channels [3,4]. Thus, the properties initiated from the collective behaviors of particles may appear unlike the effects from constituent individuals. Having a hexagonal lattice, Na$_2$OsO$_4$ is comparable to stoichiometrically equivalent Ca$_2$IrO$_4$ [5], but the magnetic and electrical measurements revealed its electrically semiconducting and non-magnetic behavior. This result notably contradicted expectations, given that Os has a 5d^2 electronic configuration, which usually leads to unpaired spin moments and some contributions from orbital moments. The absence of magnetic moments was examined experimentally, and a remarkable distortion of the OsO$_6$ octahedra was found, even though Os^{6+} is not strongly Jahn—Teller active [2,6]. Thus, it became clear that the degeneracy of the 5d_{xy} and 5d_{yz} (5d_{zx}) orbitals is broken, and Na$_2$OsO$_4$ is magnetically silent in its ground state because of spin pairing ($S = 0$). This fact was also supported using *ab initio* electronic structure calculation [1]. The scientifically intriguing aspect is that the energy gap (E_g) in such a simple system is triggered by the axial compression of the OsO$_6$ octahedra with a negligible role of SOC.

* Corresponding author.
** Corresponding author.
E-mail addresses: raimundas.sereika@hpstar.ac.cn (R. Sereika), yang.ding@hpstar.ac.cn (Y. Ding).

Under normal conditions, in the non-distorted octahedra, the $5d$ orbitals are splitted into e_g (with d_{z^2} and $d_{x^2-y^2}$ two orbitals being degenerate) and t_{2g} (with d_{xy}, d_{yz}, and d_{zx} three orbitals being degenerate). The two $5d$ electrons fill into t_{2g} orbital with two parallel spins according to the Hund's rules. This configuration gives a total local spin = 1 for each OsO_6 octahedral site. However, the octahedral distortion further splits the t_{2g} orbitals into three different energy levels, d_{xy}, d_{yz}, d_{zx}, leaving two $5d$ electrons in the lowest level (d_{xy}) with a pair of antiparallel spins. Correspondingly, the total local spin = 0, which is magnetically the silent state for each OsO_6 octahedral site in Na_2OsO_4. At high pressure, once the e_g and t_{2g} orbitals become overlapped, the two $5d$ electrons are no longer confined in the t_{2g} orbitals but become delocalized into the both e_g and t_{2g} orbitals; then, the total local spin is decreased and form a band-like magnetism. Because the magnetically silent state was directly related to the OsO_6 octahedra, physical or chemical pressure may render a significant impact on the structure by removing the OsO_6 distortion that exists at normal conditions. During compression, narrow E_g semiconductors usually switch to metals, and the non-magnetic $S = 0$ state could transform to a magnetic $S = 1$ state because the OsO_6 distortion can be removed or suppressed by pressure [7,8]. To search for the predicted quantum state, we combined high-pressure electrical transport, synchrotron X-ray absorption (XAS), and X-ray diffraction techniques (XRD) in line with first principles calculations to study the electronic and crystal structure at high pressure comprehensively. Contrary to expectations, however, we discovered that Na_2OsO_4 becomes increasingly insulating up to the 11 GPa and then gradually transforms into a metallic state at 23 GPa. According to our theoretical modeling, we concluded that the increased insulating state originates from the pressure-enhanced distortion of the OsO_6 octahedra up to 11 GPa, which is also responsible for the unusual changes observed in the electrical transport and XAS experiments.

Fig. 1 shows the temperature-dependent electrical transport properties of Na_2OsO_4. The $R(T)$ curves represent semiconducting behavior up to ~ 23 GPa (see Fig. 1a and data given in the Supporting Information). However, in this range, the activation energy (ε_T) deduced from the slope of the linear part of the electrical resistance for higher temperature region indicates non-linear curve (Fig. 1b and Fig. S4). The $\varepsilon_T(P)$ shows a maximum at 11 GPa, distinctly manifesting anomalous behavior at this pressure. Furthermore, at very low temperatures (from ~6.3 K), the conductance (G) exhibits clear power-law behavior, $G \propto T^\alpha$, which refer to the Luttinger liquid or 1-D Wigner crystal formation typical for 1-D systems (Fig. 1c and d). Therefore, we postulate that the observed phenomenon at low temperatures originates from the domain, which in turn causes the tunneling effect among different Luttinger liquids.

It is worth mentioning that the power-law does not extend to all temperature as pressure increases, as seen in some nanomaterials [9,10]. The obtained exponential values α were also relatively small ranging near 0 (see Fig. 1c and d). The compression rapidly decreased α following a polynomial trend where the power-law in metallic state (pressures > 23 GPa) appeared to be with an opposite sign (Fig. 1e). As mentioned previously, the interacting fermions in one spatial dimension do not obey FL theory; however, the possibility of the deconfinement transition induced by interchain hopping [11] or a transition to a weakly disordered FL [12] for more higher pressures cannot be neglected as α alters with pressure strongly toward the FL state. Thus, such unique behavior at low temperature and high pressure can be further addressed by using more specific techniques.

For the underlying mechanisms at room temperature and specifically at 11 GPa, we carried out X-ray absorption near edge structure (XANES) measurements. Fig. 2a and b show the Os $L_{3,2}$-edges captured at room temperature up to 28 GPa, respectively. The white-line (WL) energy position of Na_2OsO_4 Os L_3-edge
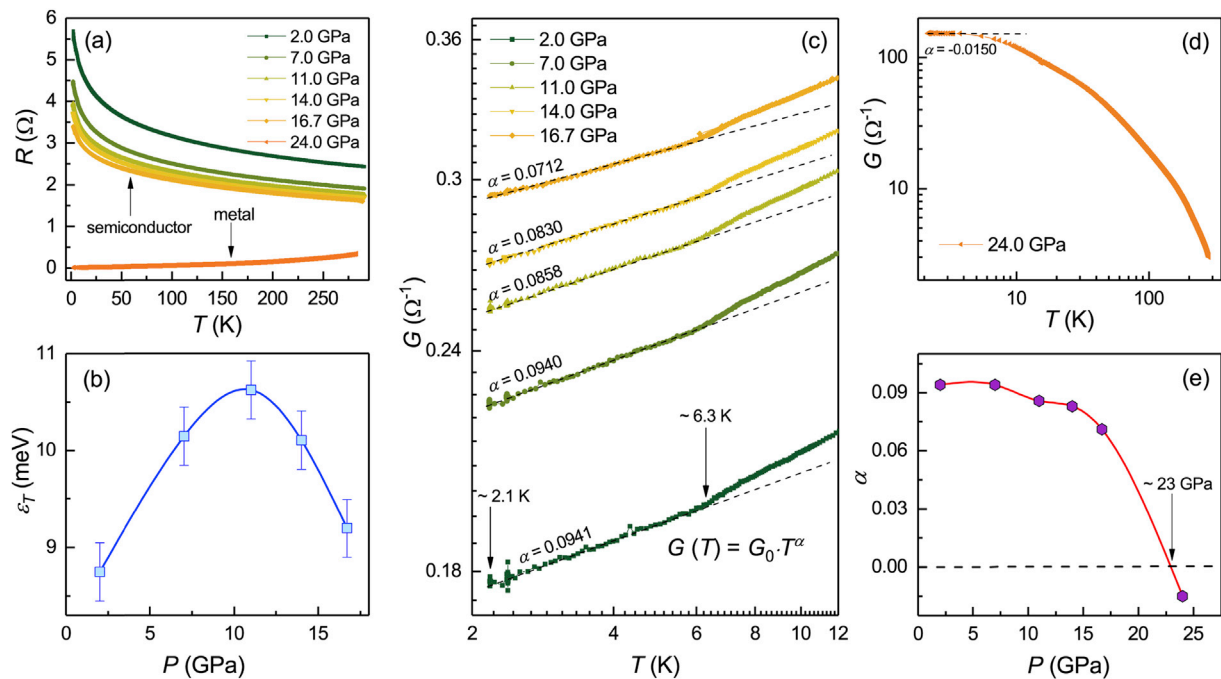

Fig. 1. The temperature-dependent electrical transport at fixed pressures. (a) Temperature dependence of the resistance (R) at various pressures. (b) The activation energy (ε_T) as a function of pressure (P) extracted from higher temperature region of the electrical transport. (c) and (d) represent log–log plots of the conductance (G) vs. temperature for semiconducting and metallic states, respectively. The power-law behavior observed at low temperatures is indicated by dashed lines, together with an exponent parameter α at each pressure. (e) The exponent α dependence on pressure where the red curve is a guide to the eye. Here, the 0 value is crossed at around 23 GPa.
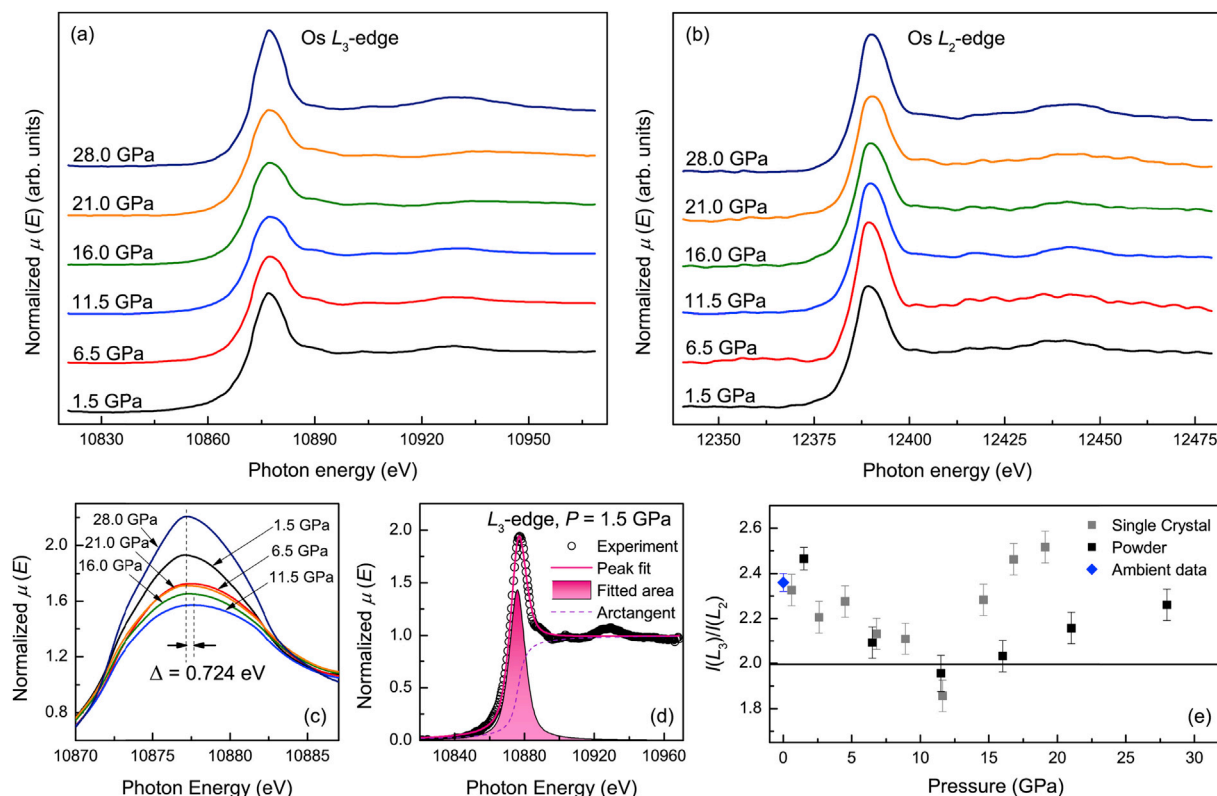
Fig. 2. The XANES data of Os L_3- and L_2-edges in Na_2OsO_4 at various pressures. (a) and (b) Evolution of the absorption spectra in a wide energy range during sample compression up to 28 GPa for the Os L_3- and L_2-edges, respectively. (c) A comparison of the L_3-edge apex from (a) plot. (d) The determination of the white-line intensity at selected pressures. The open circles are the experimental results of the normalized $\mu(E)$ coefficient at the L_3 absorption edge, while the solid pink curve represents the best fit to the data using pseudo-Voigt and arctangent fit functions. The filled area under the curve is the 'fitted area' and corresponds to the white-line intensity. The arctangent fit function is shown as the dashed line and is used to model the continuum step at the current absorption edge. It is notable that the μ(E) data were normalized so that the continuum step (the height of the high-energy plateau) at the L_3-edge is equal to unity for each pressure. Accordingly, the continuum step at the L_2-edge has been normalized to half of this value (the adopted normalization scheme is the same applied to the iridium-based 5d compounds in Ref. [15]). (e) Experimentally observed branching ratios between integrated intensities of the L_3 and L_2 absorption edges. The solid line at the ratio $I(L_3)/I(L_2) = 2$ corresponds to $\langle \mathbf{L} \cdot \mathbf{S} \rangle = 0$.

corresponded well to the $5d^2$ samples [13,14], confirming the Os^{6+} valence state at ambient pressure. Nevertheless, both the L_3 ($2p_{3/2}$ → $5d$) and L_2 ($2p_{1/2}$ → $5d$) absorption edges showed significant and unusual changes during compression. The intensity of the WL at the L_3 manifested a strong decrease during compression from 1 bar to 11.2 GPa and a strong increase from 11.2 GPa to 28.0 GPa (see Fig. 2c). The L_2 absorption edge did not indicate such a significant intensity change.

The changes under compression were also noticed in the Os WL position at the L_3 edge (Fig. 2c). The WL shift was observed in Na_2OsO_4 powders, which is also confirmed by measuring several single crystals with appropriate thicknesses. The WL shifts gradually to higher energies while under pressure up to 11.2 GPa and then reverts to its original position if more pressure is applied. As the WL position defines the valence, its shift to higher energies indicates its increase. A spectral shift at the Os L_3 edge of approximately 1.0(1) eV to higher energy indicates an increase of valence by 1+ state [14]. Based on this fact, we consider the increase of the Os valence (according to the WL position shift from powder data) from 6+ to 6.724+ during compression from 1 bar to 11.2 GPa and vice versa, a decrease of Os valence from 6.724+ to 6+ during further compression from 11.2 GPa to 28 GPa. The increase and decrease of the Os valence might be associated with the OsO_6 octahedral deformation as it is known that there is an inverse relationship between the extent of the edge energy and the average bond length [16,17].

Meanwhile, the integrated intensities $I(L_3)$ and $I(L_2)$ of the WL for each pressure were extracted from the raw data, as shown in Fig. 2d. It is known that the ratio $I(L_3)/I(L_2)$ (also called branching ratio [BR]) for 5d transition metal oxides increases with electron occupancy, and for a small electron number, the BR is less affected by SOC [18]. However, the BR is related to the ground state expectation value of the angular part of the spin-orbit coupling, $\langle \mathbf{L} \cdot \mathbf{S} \rangle$. Therefore, in the 5d manifold, $\langle \mathbf{L} \cdot \mathbf{S} \rangle = n_h(BR - 2)/(BR + 1)$, where n_h is the number of empty holes [19]. As is common, the $\langle \mathbf{L} \cdot \mathbf{S} \rangle$ barely changes within low pressure; therefore, it indicates that the electron-hole density (or electron occupancy) increases (or decreases). These results are consistent with the WL position measurements.

In addition to the XAS, we also investigated the structural changes at high pressure using diffraction methods; the results are shown in Fig. 3. There are no observable symmetry changes in the diffraction patterns up to 35 GPa in agreement with our optical measurements (for more details see Supporting Information). However, our structural refinement reveals that the OsO_6 octahedral distortion remains at high pressure and even increases with pressure up to 11 GPa, preserving $S = 0$ state. Although this particular pressure range corresponds with the solidification of neon gas at ambient temperature, the transition is consistent with the measurements performed by using other pressure mediums. The evolution of the traced osmium − oxygen bond lengths under high pressure is shown in Fig. 3b−d. During compression up to 11 GPa, the atoms O1 and O2 moved away from the osmium, giving
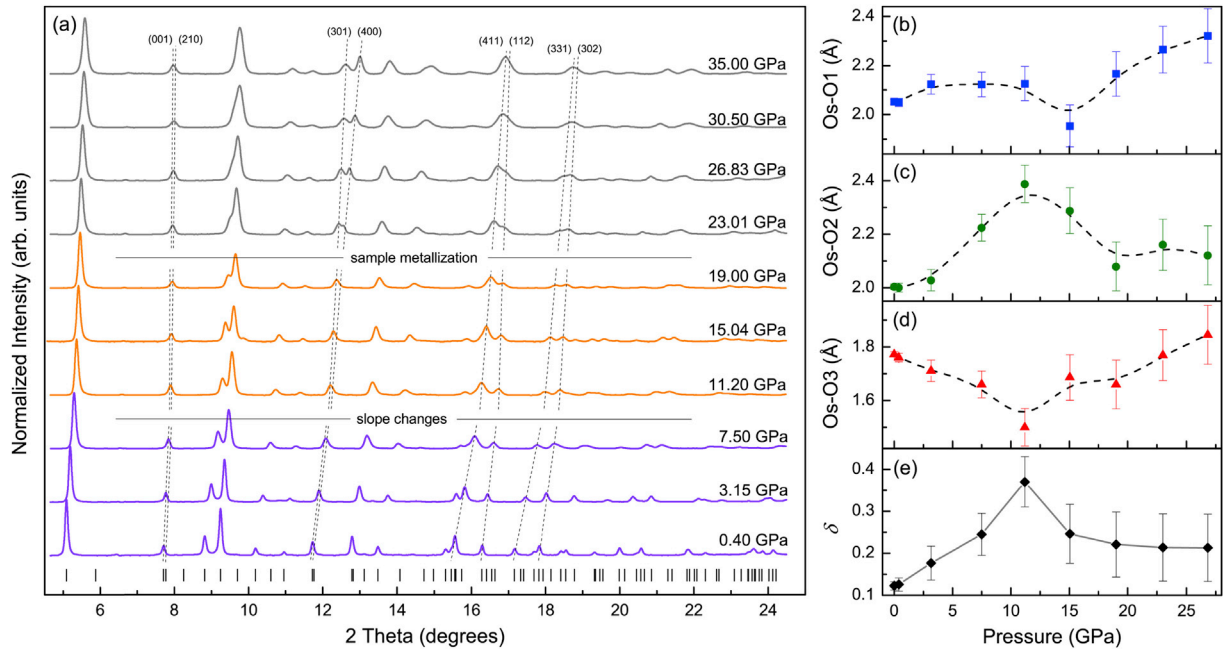
Fig. 3. Synchrotron X-ray diffraction data collected for Na_2OsO_4 powders at room temperature. (a) Evolution of diffraction patterns over sample compression (dashed lines are guides to the eye for randomly selected peaks to highlight structural changes). The XRD peaks move quickly to the higher 2θ angle up to 11 GPa. Furthermore, above 11 GPa, peaks move more slowly, which is different for some peaks, indicating that lattice parameters have different compressibility under pressure. The change in color over pressure denotes the change between different sample states. The positions of the $P\bar{6}2m$ Bragg reflections are marked by vertical bars. (b), (c) and (d) represents variations of the Os-O1, Os-O2, and Os-O3 bond lengths δ with pressure, respectively. The dashed lines are B-splines used to fit experimental data. (e) The calculated OsO_6 octahedral distortion parameter δ vs. pressure.

bond distances of 2.126 Å (Os-O1) and 2.388 Å (Os-O2), respectively. Meanwhile, the O3 atoms were found to move continuously closer to the osmium. The Os-O3 bond length reaches the minimum with a very low value of approximately 1.5 Å at 11 GPa. Further compression above 11 GPa showed opposite behavior of all the atoms, and the difference in the octahedral bonds was always greater than that at the ambient conditions. The distortion in the OsO_6 site was characterized at selected pressures by calculating octahedral strain tensor parameter δ according to the following equation [20]:

$$\delta = \sqrt{\frac{1}{n}\sum_{i=1}^{n}(d_i - d)^2} \tag{1}$$

Here, d is the average bond length, d_i is the individual bond length, and n is the number of bonds in the octahedra. The parameter δ indicates the degree of distortion away from the regular octahedron ($\delta = 0$). The larger the value of δ, the more the distortion of the OsO_6 (similarly, the defined equivalent equation—called bond-length distortion [21]—can also be used in this case). At ambient pressure, Na_2OsO_4 has $\delta = 0.122$ distortion, which is considerably greater than the isostructural Ca_2IrO_4, $\delta = 0.038$. However, we found that δ increases strongly with pressure until 11 GPa. Further increase of pressure forces distortion to drop and proceed with more or less a stable value $\delta = 0.2 \pm 0.02$.

Finally, to understand the interplay among the lattice, charge, and orbitals, we performed first-principles calculations based on the density functional theory. The structural data obtained from the diffraction measurement were used for the calculations. The pressure-dependent orbital resolved partial density of states (P-DOSs) foremost confirms that E_g is opened at the Fermi level (E_F) between d_{xy} and $d_{yz} - d_{zx}$ of the t_{2g} band (see Fig. 4). This indicates that Na_2OsO_4 is characteristic of a narrow band-gap insulator (or semiconductor), rather than a Mott insulator. The low-lying d_{xy}

states due to the distorted OsO_6 are fully occupied by two electrons, which is also consistent with the non-magnetic configuration. When the pressure increases, the d_{yz}, and d_{zx} bands move toward high energy, whereas the d_{xy} band moves toward lower energy; this enlarges the band gap (the extracted activation energy follows this trend similarly), which reaches a maximum at 11 GPa. This result explains why the Na_2OsO_4 becomes more insulating at high pressure and the E_g reaches its maximum at 11 GPa. At the same time, the electron occupancy of the d_{xy} band decreases with pressure. Such a reduction of the electron occupancy in the t_{2g} band of Os explains why the WL of L_3 edge shifts to higher energy in the XANES spectra and why the BR decreases with pressure reaching a minimum at 11 GPa.

In addition to the change in the t_{2g} band, the e_g band split into d_{z^2} and $d_{x^2-y^2}$. When the pressure increases, the $d_{x^2-y^2}$ band moves toward lower energy, while the d_{z^2} moves in the opposite direction. However, when the pressure goes beyond the 11 GPa, all the bands reverse their directions and eventually the d_{xy} and $d_{yz} - d_{zx}$ merge together closing the E_g, which results in a metallic state at 23 GPa. This result finally explains why Na_2OsO_4 becomes more insulating up to 11 GPa but then gradually turns into a more metallic state and eventually turns into a metal at 23 GPa. The band structure calculations successfully reproduce the observations, basically indicating that the electronic structure of Na_2OsO_4 at high pressure is governed by the structure, especially the distortion of OsO_6. Na_2OsO_4 could have several more features in metallic phase, which are significant for low dimensions, such as the Kondo effect [22], electron fractionalization [23,24], or superconductivity at very low temperature, $T_c < 2$ K [25].

Experimental and computational methods

The Na_2OsO_4 single crystals were obtained using the high-pressure apparatus and route described in Ref. [2]. The average crystal size was 0.1–0.3 mm, and the shape was needle-like and
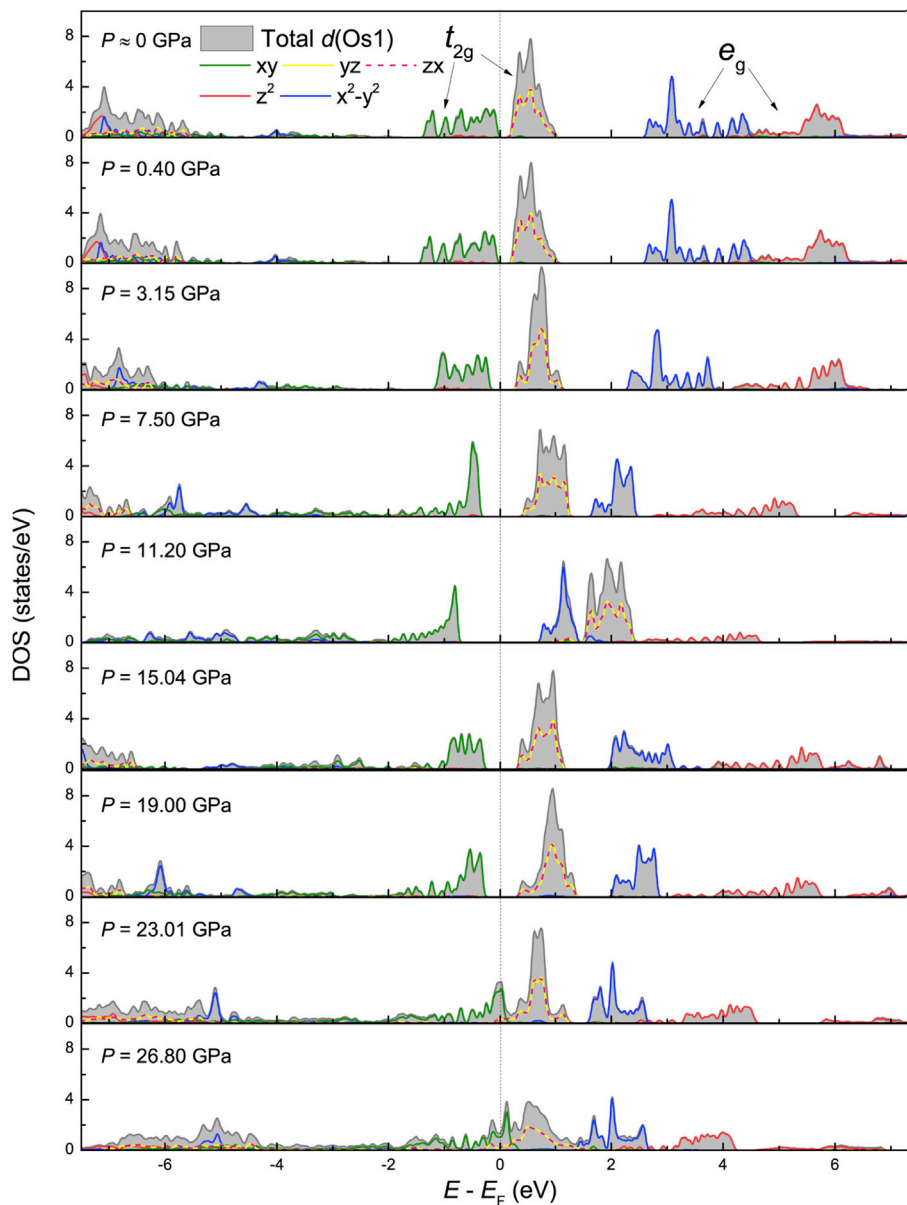
Fig. 4. The partial density of states for the Os1 atom (with consideration of its local axis) in Na_2OsO_4. For other Os atoms, the P-DOSs are just the same considering their own local axis. The t_{2g} bands at ambient pressure (marked here as $P \approx 0$) originate in the region from -1.4– 1.05 eV, and e_g bands lay in the conduction band from 2.6 to 7.4 eV. The narrow gap is opened at the top of the valence band in the t_{2g} structure. The E_F is denoted by the dotted line. The P-DOS of the d_{yz} orbital exactly matches the P-DOS of the d_{zx} orbital. P-DOS, partial density of states.

black in color. Before using the crystals, after washing several times with an ultrasonic bath, XRD test was carried out using Cu $K\alpha$ radiation in SmartLab, RIGAKU to confirm no damage.

A Mao-type symmetric diamond anvil cell (DAC) with 400 μm culet sized anvils was used for the Raman and high-pressure XRD experiments. A stainless steel gasket was precompressed to a 35 μm thickness, and a hole of 150 μm was drilled to load the sample, a ruby for pressure determination, and neon gas to serve as a pressure-transmitting medium [26]. The Raman spectra up to ~40 GPa were measured on a Renishaw inVia spectrometer with a 488 nm laser wavelength. The data collection time was 90 s and laser power of 15 mW was maintained for each spectrum. The *in situ* high-pressure XRD measurements were carried out in an angle-dispersive mode at beamline 16-BM-D of the Advanced Photon Source (APS), Argonne National Laboratory. The incident

monochromatic X-ray beam energy was set to 29.2 keV ($\lambda = 0.4246$ Å), where the sample-detector distance was 318 mm. The wavelength of the X-ray was periodically calibrated using a CeO_2 standard. Diffraction patterns were recorded on a MAR345 image plate and then integrated using DIOPTAS software [27]. Indexing and Rietveld refinements were carried out in EXPO2014 [28] and GSAS-II [29].

High-pressure XAS experiments were performed for osmium by investigating the XANES at beamline 20-BM-B of the APS. A panoramic DAC with 400 μm diamonds was used to collect spectra at both the L_2 and L_3 absorption edges for the Na_2OsO_4 powders. To avoid contamination of the XANES spectra by Bragg peaks from the diamond anvils, XANES measurements were performed in transmission geometry where the X-ray beam goes through a beryllium gasket. The gasket was initially precompressed to ~70 μm, and then

the whole culet area was drilled and replaced by boron nitride (BN) powder, which was compressed again to make a 60 μm radius hole drilled at the center of the BN insert. The sample, together with a ruby sphere and mineral oil (ACROS Organics™) as a pressure medium, were then all loaded into the prepared hole. The XANES spectra were double checked by measuring the Na_2OsO_4 single crystals. In these measurements, we used a symmetric DAC with nanodiamond anvils. A stainless steel gasket was used to make a hole for a sample, ruby, and mineral oil. The collected data were processed and analyzed using programs from the Demeter package [30].

The electronic transport properties under high pressure and low temperature were investigated via the four-probe electrical conductivity method in a DAC made of CuBe alloy. The pressure was generated by a pair of diamonds with a 300-μm diameter culet. A gasket made of stainless steel was pressed from a thickness of 250 μm to 30 μm. A hole in the center of the gasket was then drilled with a diameter of 200 μm. Fine cubic BN powder were used to cover the gasket to protect the electrode leads insulated from the metallic gasket. The electrodes were slim Au wires with a diameter of 18 μm. A 100 μm-diameter center hole in the insulating layer was used as the sample chamber. NaCl powder was used as the pressure-transmitting medium. A thermocouple was mounted near the diamond in the DAC to monitor the exact sample temperature. The measurements were performed using the Mag Lab system, which controls the temperature automatically. The pressure was measured via the ruby fluorescence method at room temperature before and after cooling. It is worth mentioning that in all the experiments, the pressure value is the average value determined before and after the measurement. In all cases, the error does not exceed ±0.5 GPa.

Electronic structure calculations were performed by the OpenMX software package [31], which is based on the linear combination of pseudo-atomic-orbital basis formalism. The exchange-correlation energy was calculated within the local density approximation functional [32]. Spin-orbit coupling was treated in the fully relativistic j-dependent pseudopotential and non-collinear scheme [33]. The $6 \times 6 \times 12$ Monkhorst-Pack k-point grid and the 400 Ry energy cut-off were used for momentum-space and the real-space integration. The theoretical calculation for the band gap verification was also performed for the volume optimized cell following a similar approach applied earlier on the Na_2OsO_4 sample [34]. Calculations were double checked with the full-potential linearized augmented plane wave method as implemented in the Wien2k software along with the Perdew-Burke-Ernzerhof parameterized generalized gradient approximation [35]. The Rk_{max} was set to 7 (R is the radius of the smallest muffin-tin sphere, and k_{max} is the largest k vector in the plane wave expansion). A mesh of 729 k-points in the irreducible part of the Brillouin zone was used. The iteration halted when the criterion for the difference in the eigenvalues was less than 0.0001 between the steps of convergence.

Appendix A. Supplementary data

Supplementary data to this article can be found online at https://doi.org/10.1016/j.mtphys.2018.12.001.

Data availability statement

The raw data required to reproduce these findings are given in the Appendix.

References

[1] Y.G. Shi, Y.F. Guo, S. Yu, M. Arai, A.A. Belik, A. Sato, K. Yamaura, E. Takayama-Muromachi, T. Varga, J.F. Mitchell, High-pressure crystal growth and magnetic and electrical properties of the quasi-one dimensional osmium oxide Na_2OsO_4, J. Solid State Chem. 183 (2010) 402—407. https://doi.org/10.1016/j.jssc.2009.12.007.

[2] K. Yamaura, Short review of high-pressure crystal growth and magnetic and electrical properties of solid-state osmium oxides, J. Solid State Chem. 236 (2016) 45—54. https://doi.org/10.1016/j.jssc.2015.06.037.

[3] J. Voit, One-dimensional Fermi liquids, Rep. Prog. Phys. 58 (1995) 977—1116. https://doi.org/10.1088/0034-4885/58/9/002.

[4] V.V. Deshoande, M. Bockrath, L.I. Glazman, A. Yacoby, Electron liquids and solids in one dimension, Nature 464 (2010) 209—216. https://doi.org/10.1038/nature08918.

[5] F.J.J. Dijksma, J.F. Vente, E. Frikkee, D.J.W. IJdo, The structure of a calcium deficient hexagonal calcium iridium oxide compound, Mater. Res. Bull. 28 (1993) 1145—1151. https://doi.org/10.1016/0025-5408(93)90094-T.

[6] R. Janes, E. Moore, Metal—ligand Bonding, Open University, United Kingdom, 2004.

[7] J. Ruiz-Fuertes, A. Segura, F. Rodriguez, D. Errandonea, M.N. Sanz-Ortiz, Anomalous High-Pressure Jahn-Teller Behavior in $CuWO_4$, Phys. Rev. Lett. 108 (2012) 166402. https://doi.org/10.1103/PhysRevLett.108.166402.

[8] F. Hong, B. Yue, N. Hirao, G. Ren, B. Chen, Ho-K. Mao, Pressure-induced iso-structural transition in a distorted perovskite via octahedron reconfiguration, Appl. Phys. Lett. 109 (2016) 241904. https://doi.org/10.1063/1.4972303.

[9] M. Monteverde, M. Núñez-Regueiro, Pressure Control of Conducting Channels in Single-Wall Carbon Nanotube Networks, Phys. Rev. Lett. 94 (2005) 235501. https://doi.org/10.1103/PhysRevLett.94.235501.

[10] F. Morales, M. Monteverde, M. Núñez-Regueiro, Pressure variation of Luttinger liquid parameters in single wall carbon nanotubes networks, Eur. Phys. J. B 65 (2008) 511—514. https://doi.org/10.1140/epjb/e2008-00364-9.

[11] S. Biermann, A. Georges, A. Lichtenstein, T. Giamarchi, Deconfinement Transition and Luttinger to Fermi Liquid Crossover in Quasi-One-Dimensional Systems, Phys. Rev. Lett. 87 (2001) 276405. https://doi.org/10.1103/PhysRevLett.87.276405.

[12] M. Bell, A. Sergeev, J.P. Bird, V. Mitin, A. Verevkin, Crossover from Fermi Liquid to Multichannel Luttinger Liquid in High-Mobility Quantum Wires, Phys. Rev. Lett. 104 (2010) 046805. https://doi.org/10.1103/PhysRevLett.104.046805.

[13] R. Morrow, J. Yan, M.A. McGuire, J.W. Freeland, D. Haskel, P.M. Woodward, Effects of chemical pressure on the magnetic ground states of the osmate double perovskites $SrCaCoOsO_6$ and Ca_2CoOsO_6, Phys. Rev. B 92 (2015) 094435. https://doi.org/10.1103/PhysRevB.92.094435.

[14] H.L. Feng, S. Calder, P.M. Ghimire, Y.-H. Yuan, Y. Shirako, Y. Tsujimoto, Y. Matsushita, Z. Hu, C.-Y. Kuo, L.H. Tjeng, T.-W. Pi, Y.-L. Soo, J. He, M. Tanaka, Y. Katsuya, M. Richter, K. Yamaura, A Dirac-Mott insulator with ferromagnetism near 100 K, Phys. Rev. B 94 (2016) 235158. https://doi.org/10.1103/PhysRevB.94.235158.

[15] J.P. Clancy, N. Chen, C.Y. Kim, W.F. Chen, K.W. Plumb, B.C. Jeon, T.W. Noh, Y.-J. Kim, Spin-orbit coupling in iridium-based 5d compounds probed by x-ray absorption spectroscopy, Phys. Rev. B 86 (2012) 195131. https://doi.org/10.1103/PhysRevB.86.195131.

[16] G. Bunker, Introduction to XAFS: A Practical Guide to X-ray Absorption Fine Structure Spectroscopy, Cambridge University Press, New York, 2010.

[17] Y.-F. Han, K. Ramesh, L.W. Chen, F.X. Chen, A. Borgna, X-ray absorption spectroscopy study of Mn_2O_3 and Mn_3O_4 nanoparticles supported on mesoporous silica SBA-15, Adv. Synchrotron Radiat. 1 (2008) 67—78. https://doi.org/10.1142/S1793617908000112.

[18] D.-Y. Cho, J. Park, J. Yu, J.-G. Park, X-ray absorption spectroscopy studies of spin−orbit coupling in 5d transition metal oxides, J. Phys. Condens. Matter 24 (2012) 055503. https://doi.org/10.1088/0953-8984/24/5/055503.

[19] D. Haskel, G. Fabbris, M. Zhernenkov, P.P. Kong, C.Q. Jin, G. Cao, M. van Veenendaal, Pressure Tuning of the Spin-Orbit Coupled Ground State in Sr_2IrO_4, Phys. Rev. Lett. 109 (2012) 027204. https://doi.org/10.1103/PhysRevLett.109.027204.

[20] Y.S. Zhao, D.J. Weidner, J.B. Parise, D.E. Cox, Thermal expansion and structural distortion of perovskite — data for NaMgF3 perovskite. Part I, Phys. Earth Planet. In. 76 (1993) 1—16. https://doi.org/10.1016/0031-9201(93)90051-A.

[21] S. Sasaki, C.T. Prewitt, R.C. Liebermann, The crystal structure of CaGeO3 perovskite and the crystal chemistry of the GdFeO3-type perovskites, Am. Mineral. 68 (1983) 1189—1198.

[22] S. Di Napoli, M.A. Barral, P. Roura-Bas, L.O. Manuel, A.M. Llois, A.A. Aligia, Kondo physics in a Ni impurity embedded in O-doped Au chains, Phys. Rev. B 92 (2015) 085120. https://doi.org/10.1103/PhysRevB.92.085120.

[23] B.J. Kim, H. Koh, E. Rotenberg, S.-J. Oh, H. Eisaki, N. Motoyama, S. Uchida, T. Tohyama, S. Maekawa, Z.-X. Shen, C. Kim, Distinct spinon and holon dispersions in photoemission spectral functions from one-dimensional $SrCuO_2$, Nat. Phys. 2 (2006) 397—401. https://doi.org/10.1038/nphys316.

[24] J. Schlappa, K. Wohlfeld, K.J. Zhou, M. Mourigal, M.W. Haverkort, V.N. Strocov, L. Hozoi, C. Monney, S. Nishimoto, S. Singh, A. Revcolevschi, J.-S. Caux, L. Patthey, H.M. Ronnow, J. van der Brick, T. Schmitt, Spin−orbital separation in the quasi-one-dimensional Mott insulator Sr_2CuO_3, Nature 485 (2012) 82—85. https://doi.org/10.1038/nature10974.

[25] Y. Maeno, K. Yoshida, Fermi liquid properties and superconductivity of Sr_2RuO_4, Czech. J. Phys. 46 (1996) 3097—3104. https://doi.org/10.1007/BF02548115.

[26] M. Rivers, V.B. Prakapenka, A. Kubo, C. Pullins, C.M. Holl, D. Jacobsen, The COMPRES/GSECARS gas-loading system for diamond anvil cells at the Advanced Photon Source, High Pres. Res. 28 (2008) 273—292. https://doi.org/10.1080/08957950802333593.

[27] C. Prescher, V.B. Prakapenka, DIOPTAS: a program for reduction of two dimensional X-ray diffraction data and data exploration, High Pres. Res. 35 (2015) 223—230. https://doi.org/10.1080/08957959.2015.1059835.

[28] A. Altomare, N. Corriero, C. Cuocci, A. Falcicchio, A. Moliterni, R. Rizzi, EXPO software for solving crystal structures by powder diffraction data: methods and application, Cryst. Res. Technol. 50 (2015) 737—742. https://doi.org/10.1002/crat.201500024.

[29] B.H. Toby, R.B. Von Dreele, GSAS-II: The Genesis of a Modern Open-Source All-Purpose Crystallography Software Package, J. Appl. Crystallogr. 46 (2013) 544—549. https://doi.org/10.1107/S0021889813003531.

[30] B. Ravel, M. Newville, Artemis Athena, HEPHAESTUS: data analysis for X-ray absorption spectroscopy using IFEFFIT, J. Synchrotron Radiat. 12 (2005) 537—541. https://doi.org/10.1107/S0909049505012719.

[31] T. Ozaki, Variationally optimized atomic orbitals for large-scale electronic structures, Phys. Rev. B 67 (2002) 155108. https://doi.org/10.1103/PhysRevB.67.155108.

[32] D.M. Ceperley, B.J. Alder, Ground State of the Electron Gas by a Stochastic Method, Phys. Rev. Lett. 45 (1980) 566. https://doi.org/10.1103/PhysRevLett.45.566.

[33] A.H. MacDonald, S.H. Vosko, Spin-polarized relativistic exchange energies and potentials, J. Phys. C Solid State Phys. 12 (1979) 2977. https://doi.org/10.1088/0022-3719/16/20/012.

[34] S.F. Matar, G. Demazeau, N. Ouaini, Ab initio investigations of the Ca_2IrO_4-type structure as a "post-K_2NiF_4": Case study of Na_2OsO_4, Solid State Sci. 13 (2011) 1396—1400. https://doi.org/10.1016/j.solidstatesciences.2011.04.011.

[35] P. Blaha, K. Schwarz, G. Madsen, D. Kvasnicka, J. Liutz, WIEN2k An Augmented Plane Wave Plus Local Orbitals Program for Calculating Crystal Properties, Vienna University of Technology, Vienna, 2001.